Chapter 3 : Crystal structure determination of a new monoclinic phase in NiMn system in a self-assembled chessboard-like microstructure

3.1 Introduction

In the recent past, there has been a renewed interest in studying Ni-Mn alloys/intermetallics for its potential application as anti-ferromagnetic shape memory alloys [86–88]. The alloy exhibits multi-step structural phase transformation from FCC-FCT-FCO and this series of phase transformations are essential for understanding of thermoelastic martensitic transformation [89].The Ni-Mn phase diagram has been a subject of investigation for past several decades [90–92]. Numerous papers on Ni-Mn phase diagram have been published [93,94]. However, the phase diagram is considerably complicated due to the presence of several structurally complex intermetallic phases, especially in the equi-atomic region. Tsiuplakis and Kneller [90] reported eight intermetallic compounds namely, Mn_3Ni, Mn_2Ni, MnNi (η), MnNi (η′), MnNi (η″), $MnNi_2$, $MnNi_2$(high temperature), and Ni_3Mn in this system. Kaufman [94] reported the existence of five cubic solid solution phases and five intermetallic phases namely, Mn_3Ni, Mn_2Ni, MnNi, $MnNi_2$, and $MnNi_3$.Coles and Hume-Rothery [91], showed, $L1_0$ as a stable phase from room temperature to 700 °C near equi-atomic composition. The controversy extends further with some phase diagrams showing the presence of as many as five different solid phases present at various temperatures in the equi-atomic region [95].Polymorphic transformation was first witnessed at the equi-atomic composition(NiMn) at a higher temperature where disordered FCC γ-phase (cF4) transformed to ordered BCC η-phase(cP2). At slightly lower temperature, the ordered BCC η-phase transformed polymorphically to a tetragonal ordered η′-phase(tP2). TEM investigation shows that, on quenching this near equi-atomic alloy, the ordered BCC η-phase (higher temperature phase) transforms to ordered tetragonal η′-phase (room temperature phase). In this phase transformation, it turns into a finely twinned microstructure, where {111} planes have been identified as twin planes and the regularity of these twinned regions are so often that it also results in forming superstructure[96]. One of the studies on the same system deciphers that η to η′ transition in NiMn system is associated with distortion in the lattice and the electronic

structure of the alloy has a role to play[87]. Adachi et al. [97]in a separate investigation have shown that at the equi-atomic region, this alloy shows cooling rate dependent twinning on certain planes. Slowly cooled alloys showed {110} as twinning plane while water quenched alloys showed twinning occurring on {111} planes, and they also confirmed the $L1_0$ phase in the equi-atomic region at room temperature. In their CALPHAD study, Guo and Du [98] have successfully constructed the phase diagram of the Ni-Mn system, in spite of their extensive effort, the phase fields remained elusive in the equi-atomic region.

Self-assembled chessboard-like (CB) microstructure in metallic and ceramic systems has regained traction following its potential application in high-density memory storage, nanoelectronics and energy devices [99–102]. CB microstructure has been reported in several metallic [103–105] and ceramic systems [106–112]. However, the field has remained largely unexplored over its formation mechanism, kinetics of growth etc. In metallic system $L1_2$ to $L1_0$symmetry breaking transition has been observed to be the prime reason behind the evolution of CB microstructure [103,104].

In the present study, the structure of as-solidified equi-atomic NiMn alloy has been investigated through X-ray diffraction (XRD) and transmission electron microscopy (TEM) coupled with simulation. It was found that the coexistence of new ordered monoclinic and disordered tetragonal phases. While disordered tetragonal phase has been reported earlier, the ordered monoclinic phase is hitherto unreported. Additionally, in the as-solidified condition the tetragonal and the new monoclinic phase forms a self-assembled CB-like microstructure. While CB-like microstructure has been reported between $L1_o$ and $L1_2$ phases in metallic systems, a CB-like microstructure between tetragonal and monoclinic phases has not been reported before.

3.2 Experimental techniques

Equi-atomic Ni-Mn alloy was melted and cast in a vacuum induction melting (VIM) furnace under inert argon atmosphere. High purity granules of nickel (99.9%, Alfa Aesar) and manganese (99.9%, Alfa Aesar) were taken in stoichiometric proportion in a recrystallized alumina crucible and it was melted in a VIM under inert Ar atmosphere. The furnace chamber was evacuated and it was purged with Ar gas before the mixture was heated. The melting was carried out at 1080 ^oC and the melt was allowed

to homogenize for 15 minutes. The melting process was repeated for three times in order to ascertain the compositional homogenization. The induction melted alloy was sliced by a slow speed diamond saw and both sides of the slice was polished for X-ray diffraction studies. High-resolution X-ray diffraction (XRD) experiment was performed using Panalytical Empyrean diffractometer with Co-K_α radiation (~1.789 Å) with 40 kV accelerating voltage and 40 mA tube current. Samples were scanned from 10° to 130°, with a step size of 0.01° and scan rate of 5°/min. The electron transparent sample for transmission electron microscope (TEM) observation was prepared in a conventional way. The alloy was sliced, was polished to a minimal thickness and then it was electro-polished with a solution of methanol and nitric acid in 2:1 ratio at -30°C. Electropolishing was carried out till a region of electron transparency was obtained in the disc. Microscopy was carried out using a Tecnai G^2T20 LaB_6TEM operating at 200 kV. The structural analysis was done by selected area electron diffraction (SAED). While recording the SAED patterns, smallest SAD aperture was used with a camera length of 150 mm. The diffraction patterns were simulated by JEMS software. For XEDS analysis liquid nitrogen cooled SiLi detector with 30 mm^2 active area and with ultrathin Be window was used.

3.3 Results

The XRD pattern of the induction melted and as solidified NiMn alloy Figure 3.1(a) shows distinct crystalline peaks with finite broadening. Additionally, some of the peaks show asymmetric split. As the alloy is furnace cooled, it is not likely to have accumulated strain or extensive grain refinement, which might lead to peak broadening. In order to understand the asymmetricity in some of the peaks and the broadening, the XRD patterns of disordered tetragonal NiMn phase (tI2; a=2.639 Å, c=3.52 Å) and disordered cubic Ni_3Mn (cF4; a=3.593 Å) phase were simulated (Figure 1b) and were matched with the experimental pattern. The simulated patterns of both the phases match with the experimental pattern and each of the peaks in the simulated pattern fall within the broadening range of the experimental pattern. The intensity ratios also show a good match with the experimental pattern. While disordered tetragonal NiMn phase is quite possible in this alloy (ICDD: 01-071-9643), disordered cubic Ni_3Mn phase (ICDD:01-071-9645) formation in this composition range would require compositional segregation

during solidification and it will necessarily lead to the formation of a Mn-rich phase for which no evidence is present in the experimental XRD pattern. Cubic Ni_3Mn phase may also show order-disorder transformation [113]. In the present case no evidence for the presence of ordered Ni_3Mn phase is present. This requires further investigation through electron microscopy

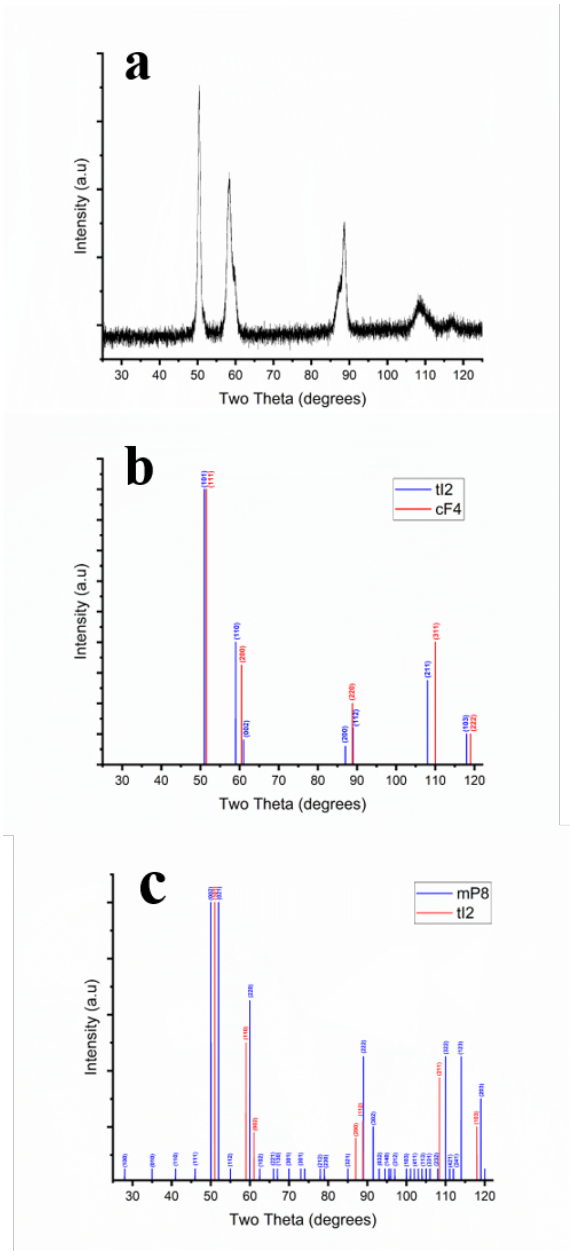

Figure 3.1: (a) Experimental x-ray diffraction pattern of the as solidified NiMn alloy (b) simulated x-ray diffraction pattern of tI2 NiMn (red) and cF4 NiMn phase (cyan) (c) simulated x-ray diffraction pattern of tI2 NiMn(red) and mP8 NiMn (cyan) phase. Both the simulated patterns show a good match with the experimental pattern.

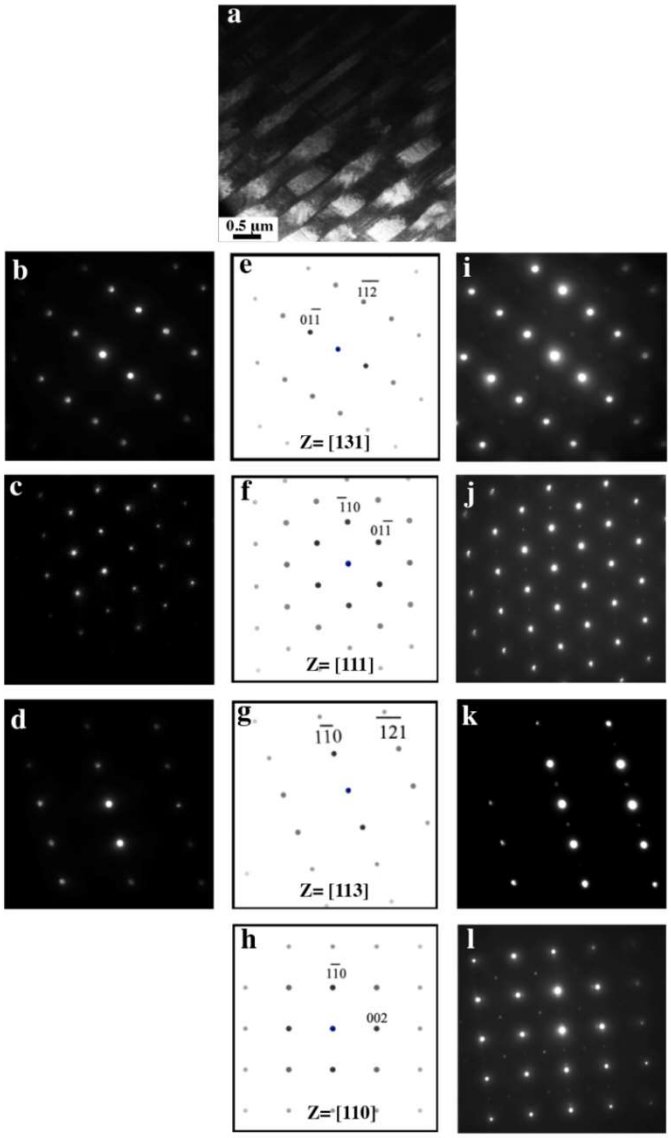

Fig 3.2:(a) TEM bright field image of the as solidified NiMn alloy in which alternative bright and dark contrast leading to a chessboard like pattern is observed. (b-d) experimental electron diffraction pattern from the bright domains along z= [131], [111] and [113] zone axes of tI2 NiMn phase, (e-h) simulated electron diffraction patterns from the tI2 NiMn phase along z= [131], [111], [113] and [110] zone axes. The simulated patterns are in scale with the experimental patterns in (b-d). (i-l) experimental electron diffraction patterns from the dark domains of the as solidified NiMn alloy. The experimental patterns show superlattice reflections along [110] and [112] directions, when compared to the simulated patterns of tI2 NiMn phase.

TEM bright field image in figure 3.2 (a) of the induction melted and as solidified alloy shows alternating bright and dark chessboard like microstructure with distinct almost straight interfaces between them. The size of the bright and dark domains varies in the range of ~200-400 nm. The diffraction patterns from different zone axes of the bright domain (Figure 3.2(b-d)) can be consistently indexed to the disordered tetragonal (I4/mmm) tI2 NiMn phase with a=2.639 Å, c=3.52 Å. The simulated electron diffraction patterns from the tI2 NiMn phase along z= [131], [111], [113] and [110] zone axes are given in Figure 3.2(e-h). The simulated diffraction patterns are in scale with the experimental diffraction patterns in Figure 3.2(b-d). The simulated diffraction pattern along z = [131], [111] and [113] zone axes show a good match. However, the diffraction patterns (Figure 3.2(i-l)) from the dark phase in Figure 3.2a cannot be indexed consistently to any of the reported phases. The diffraction patterns from the dark phase in Figure 3.2a are quite related to those from the bright phase. The diffraction patterns from the dark phase (Figure 3.2(i-l)) show superlattice reflections along <110> and <112> type directions of tI2 NiMn phase. This observation necessarily means that the bright and the dark phase might be structurally correlated, however, they are different from each other in terms of crystal structure/ordering. However, there is no signature of cubic Ni_3Mn phase in the observed microstructure.

3.4 Discussion

From the electron diffraction patterns in Figure 3.2(b-d), existence of disordered tetragonal tI2 NiMn phase is confirmed. The electron diffraction patterns in Figure 3.2(i-l) indicates that the new phase is related to the disordered tetragonal NiMn phase with additional ordering along [110] and [112] directions. In order to rationalise this observation, the lattice of disordered tetragonal NiMn phase is given in Figure 3.3(a), in which the atomic positions are decorated with average atoms of Ni and Mn. As the order is introduced along [110] direction (Figure 3.3b) periodicity along [110] direction gets doubled and it calls for introduction of order either along [100] or [010]. Schematic representation of probable atomic arrangements in the (001) plane of the new phase is given in Figure 3.3(c-d). In figure 3.3(c), ordering has been introduced along [010] direction and along [110] direction. However, it forbids order along [100] direction. Henceforth it will be referred to as “Layer A”. If order is introduced both along [100] and [010], then order cannot be maintained along [110] in figure 3.3(d), which is

contrary to the observation in the electron diffraction patterns in Figure 3.2(i-l). Henceforth it will be referred as “Layer B”. It can be concluded from this observation that the new phase is having order either along [100] or [010] and [110]. This will result in doubling of the lattice parameter of the new phase along [100] and [010] directions with respect to the disordered tetragonal tI2 NiMn phase. In order to resolve the structure of the new phase, it is required to assess the stacking of the (001) plane of the new phase along [001].

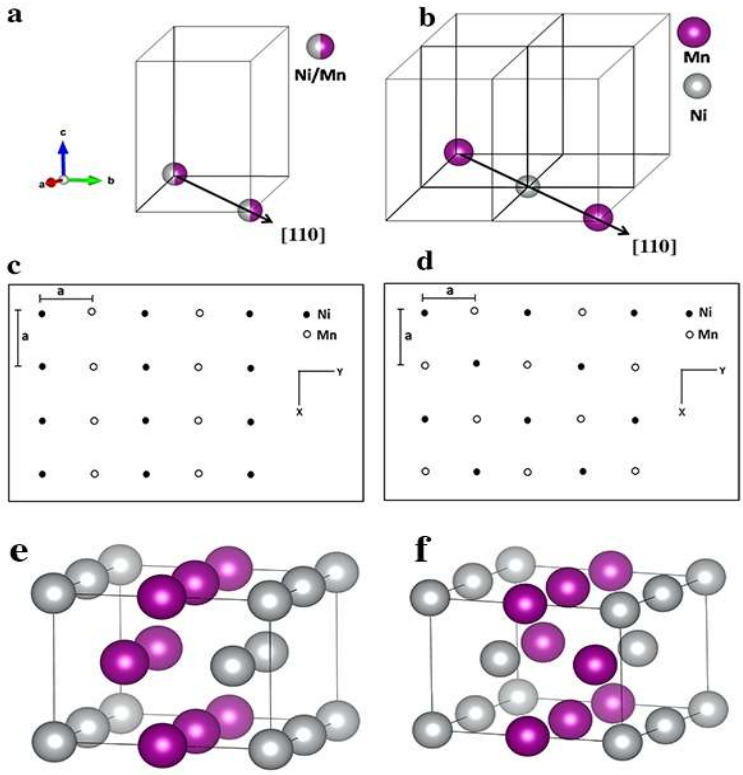

Figure 3.3. (a) Schematic representation of the disordered tetragonal lattice in which Ni and Mn atoms are shown in some of the lattice positions by average atoms. (b) schematic representation of the same tetragonal lattice in which order has been introduced along [110] direction resulting into the doubling of the lattice spacing along [110] with respect to the tI2 NiMn phase. (c) schematic representation of (001) plane in which order has been introduced along [010] and [110] (d) schematic representation of the (001) plane in which order has been introduced along [100] and [010](e) Schematic representation of Structure I, which is obtained by stacking Layer A on Layer A with a relative displacement of ¼[110] (f) schematic representation of Structure II, which is obtained by stacking Layer B on Layer A with ¼[110] relative displacement.

From the electron diffraction pattern in Figure 3.2(l), it is observed that the new phase is having order along [110] and [112]. However, it does not have any order along [002]. This necessarily means that there is no doubling of lattice parameter along [001]. However, it is required to resolve the atomic arrangements in (002) planes in order to decipher the structure further. As Layer A can only show ordering along [110], the possible stacking sequences are Layer A on Layer A (henceforth it will be referred as "Structure I") or Layer B on Layer A (henceforth it will be referred to as "Structure II") with a relative displacement of two layers by 1/4[110]. The arrangement of Layer A on Layer A results in a crystal structure, which is shown in Figure 3.3(e). The equivalent positions of the atoms in the lattice are

Ni: (0, 0, 0); (½, 0, 0); (¼,¾, ½); (¾,¾, ½)

Mn :(0, ½, 0); (½, ½, 0); (¼, ¼, ½); (¾,¼, ½)

The arrangements of Layer B on Layer A results in another crystal structure, which is shown in Figure 3.3(f). The equivalent positions of the atoms in this lattice are

Ni: (0, 0, 0);(½, 0, 0); (¼, ¾, ½);(¾, ¼, ½)

Mn: (0, ½, 0);(½, ½, 0);(¼, ¼, ½);(¾, ¾, ½)

The calculation of structure factor for the above-mentioned two structures are given in Table 3.1. It is observed from the table that when the crystal structure forms by stacking the Layer A upon Layer A with 1/4[110] displacement 001, 110, 111, 112 and 310 are the forbidden reflections. Whereas, 002, 021, 220 and 222 are allowed reflections. As in the diffraction pattern of the new phase 112 and 110 reflections are observed, possibility of this structure for the new phase is ruled out.

The structure that forms by stacking the Layer B on Layer A with 1/4[110] relative displacement, the only forbidden reflection is 001. Otherwise allowed reflections are 110, 111, 112, 002, 021, 220, 222 and 310. As the new phase shows 110 and 112 type superlattice reflections, the new phase is likely to have the structure as depicted by the stacking of Layer B on Layer A with ¼[110] relative displacement between them.

Table 3.1: Calculation of structure factor for different planes for Structure I and Structure II

	Structure I	Structure II
F_{001}	0	0
F_{110}	0	$2f_{Ni}$-$2f_{Mn}$
F_{111}	0	$2f_{Ni}$-$2f_{Mn}$
F_{002}	$4f_{Ni} + 4f_{Mn}$	$4f_{Ni} + 4f_{Mn}$
F_{021}	$4f_{Ni} + 4f_{Mn}$	$4f_{Ni} + 4f_{Mn}$
F_{112}	0	$2f_{Ni}$-$2f_{Mn}$
F_{220}	$4f_{Ni} + 4f_{Mn}$	$4f_{Ni} + 4f_{Mn}$
F_{222}	$4f_{Ni} + 4f_{Mn}$	$4f_{Ni} + 4f_{Mn}$
F_{310}	0	$2f_{Ni}$-$2f_{Mn}$

Further, to verify the model proposition of the structure, experimentally observed electron diffraction patterns from the new phase are compared with simulated electron diffraction patterns (Figure 3.4). It brings out an excellent match between the experimental diffraction patterns and the simulated patterns. and it has been found that stacking of Layer B on Layer A (structure II) with ¼[110] displacement builds the new NiMn phase. The x-ray diffraction pattern of the new NiMn phase has been simulated. The simulated x-ray diffraction patterns of the new NiMn phase along with the simulated pattern of tI2 NiMn phase are given in Figure 1c. Both the simulated pattern match with the experimental pattern in figure 3.1(a). The superlattice reflections from the new NiMn phase cannot be observed in the experimental pattern as the intensity of the superlattice reflections are quite small (Table 3.1) and they lie behind the background of the experimental x-ray diffraction pattern.

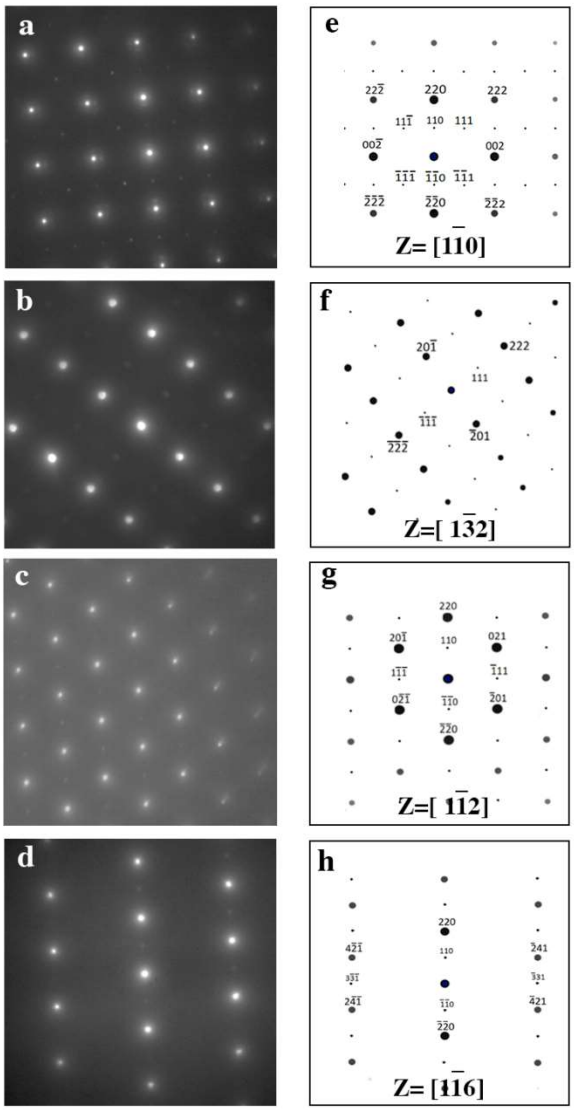

Figure 3.4: (a-d) Experimentally observed electron diffraction patterns and (e-h) corresponding simulated electron diffraction patterns from the new mP8 NiMn phase in the as solidified alloy.

The generated structure shows 2-fold symmetry along [001] and 1-fold symmetry along [100] and [010]. Experimentally observed electron diffraction patterns from different zone axes match with the simulated diffraction patterns in Figure 3.4. To rule out the possibility that the "unallowed" superlattice reflections might be from multiple scattering or double diffraction, we have simulated our signature [110] zone axis diffraction pattern incorporated with double diffraction spots. The double diffraction spots are in white circles. Had the double diffraction been taking place, all the spots

within the white circles would have been excited. However, in the experimental diffraction pattern none of such spots are observed. This led us to conclude that the extra spots are not due to double diffraction. This structure shows one 2-fold symmetry along its principal axis (unique axis c), which confirms the structure to be **monoclinic**. Convergent beam electron diffraction (CBED) pattern from the monoclinic phase is given in Figure 3.5. In the diffraction pattern, 2-fold symmetry is observed, the inversion of contrast in opposite disks necessarily confirms the presence of centre of inversion i. e. 2/m point group symmetry in the crystal. The number of atoms in the monoclinic unit cell is 8. Therefore, the Pearson symbol of the structure is **mP8** and has a space group **P 2/m,** where the coordinates (Wyckoff positions) are

Ni atoms1a (0,0,0); 1d (1/2,0,0); 2n (1/4,3/4,1/2), (3/4,1/4,1/2)

Mn atoms1b (0,1/2,0); 1e (1/2,1/2,0); 2n (1/4,1/4,1/2), (3/4,3/4,1/2)

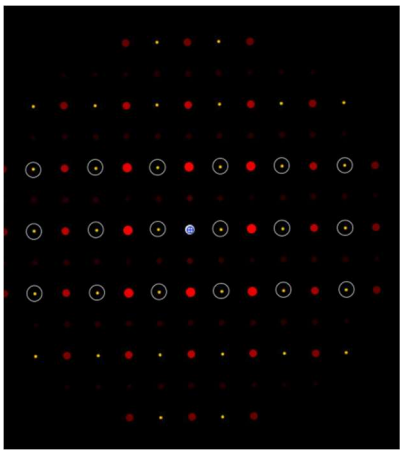

Figure 3.5 Simulated electron diffraction pattern of mP8 phase from [110] zone axis showing unallowed reflections circled in white.

The lattice parameter of these phases can be calculated from the electron diffraction patterns. The calculated lattice parameters are NiMn mP8 a=5.02 Å, b=5.16 Å, c=3.61 Å and $\alpha=\beta=\gamma=90^0$. A definite orientation relationship between the tetragonal and the monoclinic phase may be established from the diffraction pattern analysis. The orientation relationship is

$[110]_{tetragonal} \parallel [1\bar{1}0]_{monoclinic}$, $[111]_{tetragonal} \parallel [1\bar{1}2]_{monoclinic}$, $[131]_{tetragonal} \parallel [1\bar{3}2]_{monoclinic}$ and $[113]_{tetragonal} \parallel [1\bar{1}6]_{monoclinic}$

The difference in lattice parameter between the tetragonal and the monoclinic phase is likely to give rise to strain. It should be pointed out that the interface structure between the domains in the chessboard-like microstructure is not completely understood [105]. It was believed that the chessboard-like microstructures evolved in two dimension [114]. However, only recently it has been established that such type of microstructures evolves in three dimension. Additionally, it has also been pointed out that in order to reduce the strain, the domains undergo a relative rotation [112,115]. As this matter is beyond the theme of the paper, the interface structure and the interface strain between the tetragonal and the monoclinic phase would not be discussed any further.

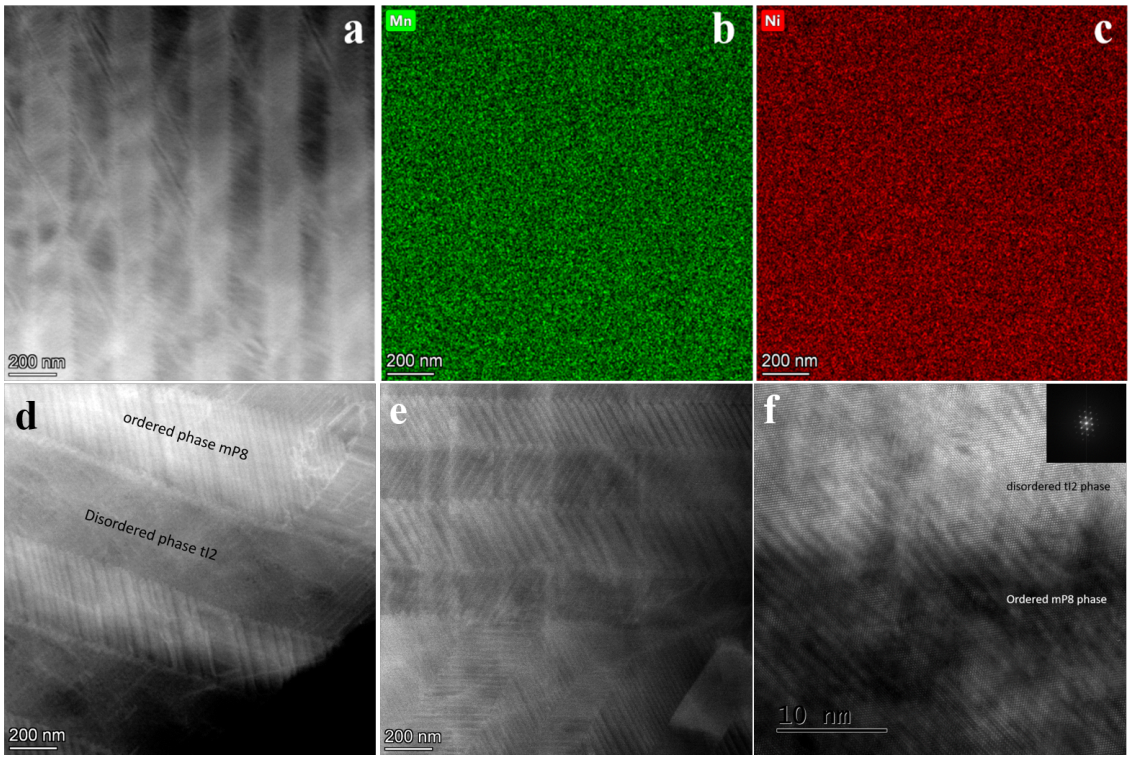

Figure 3.6:(a) HAADF image of the as solidified NiMn alloy in which alternating bright and dark contrast arising out of the two related phases can be observed. (b-c) XEDS spectral map on Ni and Mn respectively, in which no composition segregation is observed. (d) streaks in the ordered phase mP8 can be observed. (e) tweed structures in the ordered mP8 phase with different variants can be observed. (f) coherent interface at the disordered tI2 and mP8 phase can be observed.

XEDS spectral maps (Figure 3.6(b-c)) from the alloy confirms uniform composition of the NiMn alloy. In the HAADF image of the alloy in figure 3.6(a) alternate bright and dark contrast is observed, which arises due to the alternating presence of the tetragonal and the monoclinic phase. However, in the composition maps (Figure 3.6(b-c)) no composition modulation between Ni and Mn could be observed. The contrast in the HAADF image is mostly due to the existence of structural interface between the tetragonal and the monoclinic phase in the microstructure which can clearly be seen in Figure 3.6(d-e). The tweed structures can also be clearly observed which might be contribute to the mechanism of chessboard microstructures. The interface of the ordered and disordered phase is coherent and follows the orientation relationship which can further be confirmed from the phase contrast image shown in Figure 3.6 (f). As the analytical image is a differently tilted version of the chessboard-like image in Figure 3.2(a), the rod like contrast is observed. Conversion of chessboard-like microstructure to rod like microstructure at a different tilt has been observed before for other systems [27].

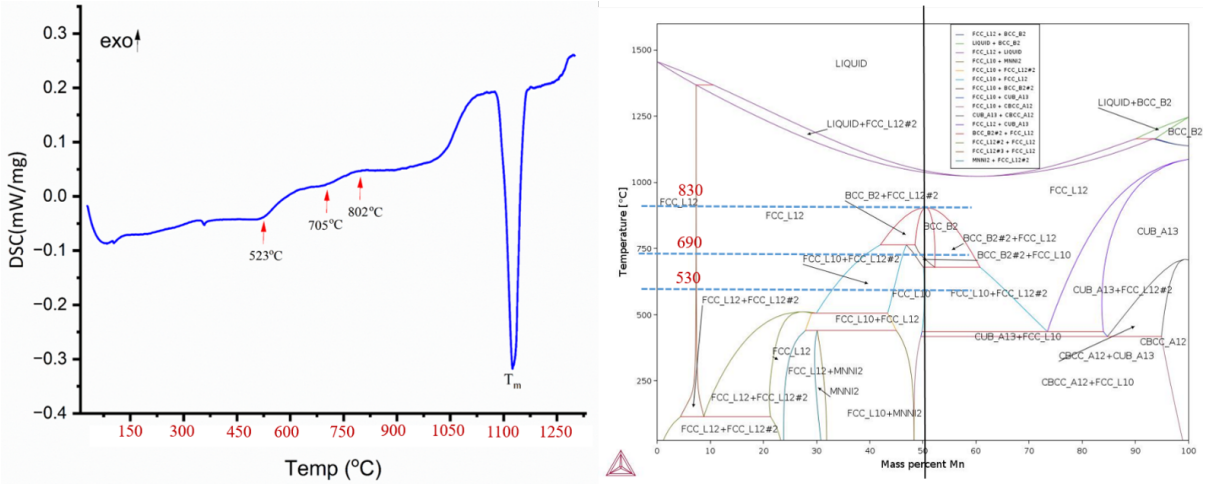

Figure 3.7: DSC thermogram of equi-atomic NiMn system showing various solid state phase transformations at 523˚C, 705 ˚C, 802 ˚C in correlation with the phase diagram.

The DSC thermogram of equi-atomic induction melted as-solidified can be observed in Figure 3.7. The profile shows various solid state phase transformation at 523˚C, 705 ˚C, 802 ˚C in correlation with the phase diagram shown adjacent to it.

Ni-Mn phase diagram being complicated especially at the lower temperature region of the phase diagram, the new ordered monoclinic phase reported in the present

study may be a metastable one. However, a profound structural correlation could be established based on its space group analysis. The space group for the already reported tetragonal phase is I4/mmm (SG# 139). One of its subgroups is P4/mmm (SG# 123), which is again tetragonal primitive. Orthorhombic subgroup of P4/mmm is Cmmm (SG# 65). Again, monoclinic subgroup of orthorhombic Cmmm is P2/m (SG# 10), which is the phase reported here. A series of symmetry breaking phase transformations may lead to the formation of the monoclinic phase from the tetragonal phase. Chessboard-like microstructures in metallic systems have been reported to be formed between tetragonal and cubic phases [103,112]. In the present study, the chessboard-like microstructure is being reported between tetragonal and monoclinic phases. It has to be emphasized here that the underlying lattice in the monoclinic phase is still tetragonal, due to motif ordering, a symmetry breaking transition takes place, which transforms the structure to monoclinic. Several theories [105,112,116] have been proposed to explain the evolution of self-assembled chessboard-like microstructures. The mechanism of chessboard-like microstructure evolution in the present case still remains to be a subject of study. It has been reported in literature that the chessboard-like microstructure may find potential applications in high-density memory storage, self-assembled solid-state batteries, self-assembled nanoscale heat pumps etc. Chessboard-like microstructure in Ni-Mn system between a monoclinic and a tetragonal phase has not been reported till date.

3.5 Conclusions

1. In the as-solidified equi-atomic NiMn alloy, along with the tetragonal η′ phase, a new monoclinic phase with P 2/m space group has been found. The lattice parameter of the mP8 phase is a=5.02 Å, b=5.16 Å, c=3.61 Å.
2. The tetragonal η′ phase and the monoclinic phase form a self-assembled chessboard-like microstructure in the as-solidified alloy.
3. In metallic systems, chessboard-like microstructure between a tetragonal and a monoclinic phase is being reported for the first time.